International Symposium
On Turbulence and Shear Flow
Phenomena (TSFP-9)
June 30 - July 3, 2015 *Melbourne, Australia*

EMPIRICAL WALL FUNCTIONS FOR MHD APPLICATIONS

Jose A. Escobar, Ismail B. Celik, Tao Yang, Albio Gutierrez
Department of Mechanical and Aerospace Engineering
West Virginia University
395 Evansdale Dr., P.O. Box 6101, Morgantown, WV, 26506, USA
ismail.celik@mail.wvu.edu

ABSTRACT

The present study reports on the development of wall functions for a channel flow where a transverse magnetic field was applied. The empirical functions proposed include both the effect of inertial forces (Reynolds number) and electromagnetic forces (Hartmann number). These wall functions were then used with the standard $k-\varepsilon$ turbulence model modified to include the influence of a magnetic field to predict the flow variables for different Reynolds and Hartmann numbers. Results using the Spalart-Allmaras (SA) turbulence model were also included in the present study for comparison. CFD simulations with the $k-\varepsilon$ model and empirical wall functions were able to predict the correct trend of the problem variables (i.e. velocity, turbulent viscosity, turbulent kinetic energy, and turbulent dissipation rate) in the fully turbulent regime, i.e. $\xi=Ha^2/Re < 0.15$.

INTRODUCTION

Magnetohydrodynamic (MHD) technology has re-emerged in recent years as an option to increase the efficiency in power generation. New concepts for power generation plants consist in the integration of oxy-coal combustors along with MHD power generators. The high exhaust gas temperature from the oxy-coal combustion along with the seeding of salts in the exhaust stream makes the gas stream suitable for MHD power generation.

In order to explore the feasibility of such integrated systems it is necessary to develop CFD (Computational Fluid Dynamics) tools that can predict the MHD generator performance.

There is considerable literature concerning CFD predictions of turbulent MHD flow, for instance Noguchi et al. (1994) reported the direct numerical simulation (DNS) results of the fully developed turbulent MHD flow for cases where the magnetic field was applied in the transverse and longitudinal direction of the flow. Noguchi et al. (1994) made available the results of the DNS calculations and can be accessed in the Internet (http://thtlab.jp/index-orig.html) for cases with a Reynolds number based on the friction velocity equal to 150 with an applied transverse magnetic field, and Hartmann number equal to 4 and 6. The website also contains cases for a Hartmann number equal to 6 and 20 where the magnetic field was applied in the longitudinal direction for a friction number of 150.

Simulations of MHD power generator using large eddy simulations (LES) for the turbulence modelling were also previously reported, e.g. Kobayashi et al. (2012). LES calculations focused on the study of the effect of the magnetic field on the flow field especially at high Hartmann number where the relaminarization (turbulence suppression) is achieved by increasing the magnetic field strength.

DNS and LES calculations are very expensive in terms of the computational time and these are not practical for industrial scale engineering problems. For this reason, in the present study the RANS model was explored using the standard wall function approach.

There are many closure models that can be used in the RANS simulations (e.g. Spalart-Allmaras, standard $k-\varepsilon$ model, etc.) which were modified in order to include the effect of the magnetic field in the turbulent quantities. Dieteker et al. (2003) proposed the modification of the Spalart-Allmaras model by changing the constant of the damping functions that is used to calculate the turbulent viscosity. The modified value of the model constant (C_{v1}) depends on the relative ratio of the Hartmann number and the Reynolds number via an empirical function.

The simulations using the SA turbulence model of turbulent MHD flow predicted reasonable results and the correct trend as the intensity of the magnetic field was varied. However, the SA turbulence model has its limitations in complex geometries (Versteeg et al., 2007) where it is difficult to define the length scale used in the destruction term. In order to overcome this limitation it was decided to explore the standard $k-\varepsilon$ turbulence model. This model is one of the most robust turbulence models used in industrial applications.

Takahashi et al., (1989) proposed modifications to include the effect of the transverse magnetic field on the turbulent quantities by including source terms in the turbulent kinetic energy and the turbulent dissipation rate equations. This particular version of the $k-\varepsilon$ model is used for studying the wall functions for MHD applications.

MODEL DEVELOPMENT

Governing Equations

The continuity, momentum and electric potential equations were solved via user defined functions (UDFs) in conjunction with the commercial CFD software ANSYS-FLUENT. The assumptions made for the current

problem are: steady state, Newtonian fluid flow, and constant fluid properties. The governing equations are

Continuity:

$$\nabla \cdot \vec{V} = 0 \tag{1}$$

Momentum:

$$\rho\left(\vec{V}\cdot\nabla\right)\vec{V} + \rho\frac{\partial}{\partial x_j}\left(\overline{u_i' u_j'}\right) = -\nabla p + \mu\nabla^2\vec{V} + \vec{F}_{Lorentz} \tag{2}$$

Electric potential:

$$\nabla^2\varphi = \nabla\cdot\left(\vec{V}\times\vec{B}\right) \tag{3}$$

Where $\vec{V}$ is the mean velocity vector, ρ is the density of the fluid, p is the mean pressure, μ is the flow viscosity, $\vec{F}_{Lorentz}$ is the Lorentz force, φ is the electric potential, $\vec{B}$ is the applied magnetic field. The Lorentz force for a moving conductor can be calculated using Equation (4)

$$\vec{F}_{Lorentz} = \vec{j}\times\vec{B} \tag{4}$$

where

$$\vec{j} = \sigma\left(-\nabla\varphi + \vec{V}\times\vec{B}\right) \tag{5}$$

is the current density vector, and σ is the electrical conductivity of the fluid. The present calculations were assumed to correspond to a low electrical conductivity where the magnetic Reynolds number is much less than one so the induced magnetic field is negligible compared to the applied magnetic field (Dieteker et al., 2003). Thus, the magnetic induction equations do not need to be solved. In the present study a constant magnetic field $\vec{B}$ is imposed on the flow field. Therefore turbulent cross correlation $\overline{j_i' b_j'}$ and $\overline{u_i' b_j'}$ are neglected.

The standard $k-\varepsilon$ turbulence model (Launder et al., 1972) was used in the present study with the modifications proposed by Tagahashi et al. (1989). The model constants are: $\sigma_k = 1.0$, $\sigma_\varepsilon = 1.3$, $C_{1,\varepsilon} = 1.44$, $C_{2,\varepsilon} = 1.92$, and $C_\mu = 0.09$. These source terms proposed by Takahashi et al. (1989) are $S_{MHD,k} = -0.8\sigma B^2 k$, $S_{MHD,\varepsilon} = -1.0\sigma B^2\varepsilon$ for k and ε equations, respectively.

Development of wall functions

The standard wall function used in flows without a magnetic field follows the usual approach (see e.g. Pope, 2000). In the current application it is somewhat generalized such that in addition to using the log-law (Eq. 6) for the velocity, the wall shear stress is calculated from $\tau_{wall} = \rho\tilde{u}_\tau u / u^+$ where $\tilde{u}_\tau = (C_\mu)^{1/4} k^{1/2}$, u is the velocity parallel to the flow. Then the production of k in the first cell is calculated using this value of τ_{wall}, and the dissipation rate is calculated as $\varepsilon = \tilde{u}_\tau^3 / \kappa y$ (see e.g. Versteeg et al. 2007). As it is well known these relations are derived by assuming local equilibrium in the log-layer (i.e. porduction of k equal to dissipation). Some concern might be raised as to the validity of this assumption for MHD cases with high Ha numbers. Indeed from the DNS simulations presented in the literature (see e.g. Kenjeres et al. 2004 and Chen et al. 2010), local equilibrium assumption is still valid for $y^+ > 20$. The logarithmic velocity profile used in the absence of magnetic field is:

$$u^+ = \frac{1}{\kappa}\ln\left(Ey^+\right) \tag{6}$$

where $u^+ = u/u_\tau$, u_τ is the friction velocity ($u_\tau = \sqrt{\tau_{wall}/\rho}$), τ_{wall} is the wall shear stress, κ is the Von Karman constant ($\kappa = 0.4187$), E is a constant ($E = 9.793$), $y^+ = yu_\tau/\nu$, ν is the kinematic viscosity.

An imposed transverse magnetic field creates a Lorentz force acting in the opposite direction of the axial flow which causes flattening of the velocity profiles near the middle of the channel. The magnetic field also affects the turbulent quantities by modifying the energy cascade by dissipating more energy mainly due to the decrease in turbulent fluctuations (Lee et al., 2001). Our preliminary investigation focused on using a relation for the nondimensional mean velocity given by an empirical which tends to hyperbolic tangent profile for high Ha^2/Re and to the classical log-law as Ha tends to zero worked much better. Some brief details of this function is given in Appendix A. The wall function values were calculated in two ways: (1) using the digitized data from Kenjeres et al. 2004, (2) using Eq. (a.1) given in Appendix A.

Here the Reynolds and the Hartmann numbers were defined as $\mathrm{Re} = UH/\nu$, and $Ha = BH\sqrt{\sigma/\mu}$, where U is the average velocity and H is the half channel height. As wall function boundary conditions, the value of u^+ was interpolated from the digitized data using a scaling factor $\xi = Ha^2/\mathrm{Re}$. An example is shown in Figure 1. The empirical wall functions developed (see Appendix A) also used ξ as the scaling factor. The ratio (Ha^2/Re) was chosen as the scaling factor because it appears naturally in the non-dimensional momentum equation (Chaudhary et al., 2011).

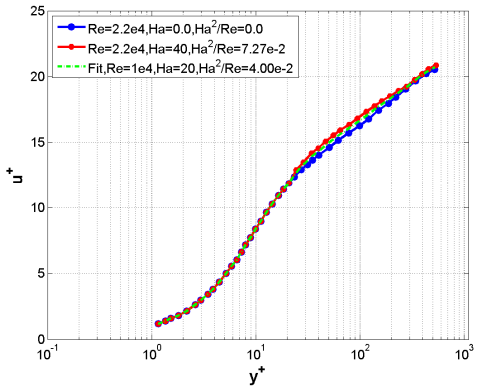

Figure 1. Interpolated velocity profile for $Ha = 20.0$ and $\mathrm{Re} = 1.0e4$.

RESULTS

First, simulations using the SA turbulence model with good near wall resolution were performed for different magnetic field intensities to study the behaviour of the mean velocity profiles along with the turbulent viscosity ratio. These were later used to develop the wall functions and to compare the results against the $k-\varepsilon$ turbulence model. The simulations were performed for a duct flow with the geometry and boundary conditions shown in Figure 2.

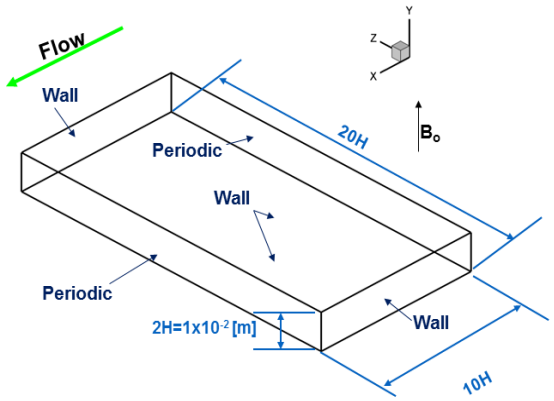

Figure 2. Domain dimensions and boundary conditions.

The main direction of the flow was in the *x*-direction while the magnetic field was applied in the *y*-direction. The non-slip boundary condition was applied at the walls of the domain and a periodic boundary condition was applied on the faces normal to the *x*-direction. The physical properties used were: ρ =1.225 [kg/m^3], σ = 800 [S/m], μ =1.8x10^{-5} [kg/(s*m)].

The initial set of calculations were performed for a turbulent duct flow with the friction Reynolds number $\mathrm{Re}_\tau = 150$ and the Hartmann numbers $Ha = 0$, and 6 .The results were compared with the DNS simulations that were previously reported by Noguchi et al. (1994). The mean velocity profiles and the turbulent viscosity profiles predicted are in good agreement with DNS results except in the wake region as shown in Figures 3. These profiles were extracted from the middle of the domain where *x* = *5H*, *z* = 0 and the profiles were plotted along the *y* direction where *y*=0 is the wall and *y/H* = 1 represents the middle of the duct. The velocity profiles were affected especially in the log-law layer and the outer layer and the turbulent viscosity ratio decreased as it was expected.

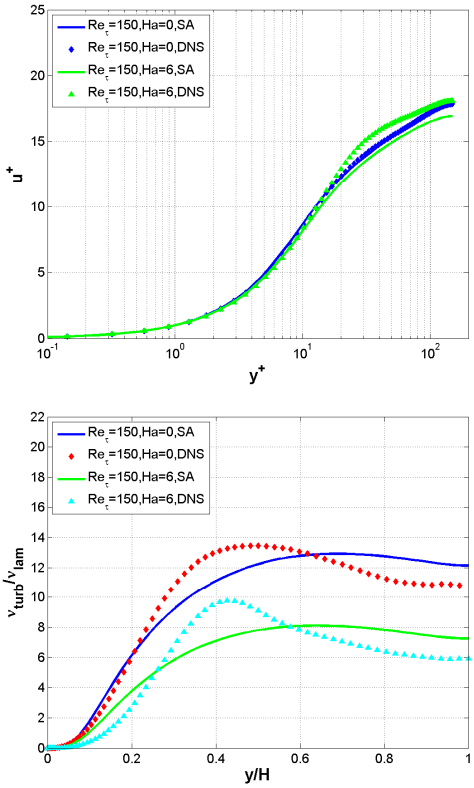

Figure 3. Mean velocity profiles (top) and turbulent viscosity ratio profile (bottom) comparison between SA and DNS (Noguchi et al., 1994) results.

Due to the low Reynolds number, Re , based on the mean bulk velocity was equal to 4710, it was decided to run another set of cases for a Reynolds number of 10,000 with different values of the Hartmann number: Ha=20 and 30. The results are shown in Figures 4.

Three dimensional simulations using the SA model predicted a flatter mean velocity profile near the center of the channel (Figure 4(top)) and the decrease of the turbulent viscosity ratio (Figure 4 (bottom)) as the magnetic field was increased. The next step in the calculations was to implement the standard $k-\varepsilon$ model

with wall functions. Three dimensional calculations of the turbulent duct flow with Re = 10,000 and Ha = 20 were performed for a mesh with a y^+ ~ 20 for the first computational cell from the wall.

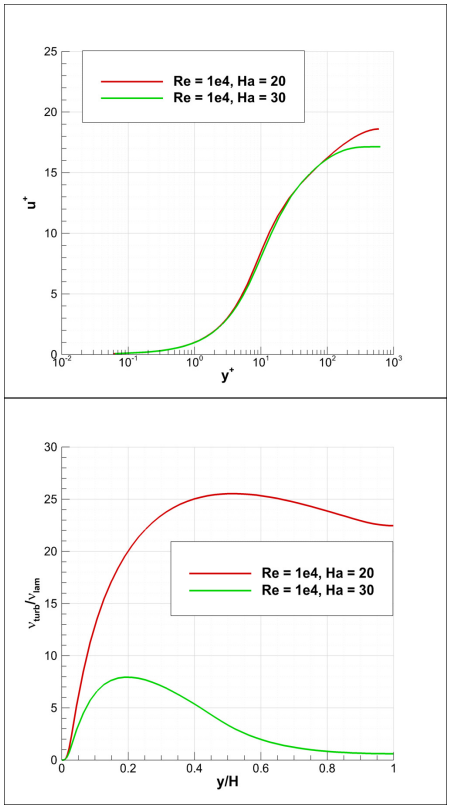

Figure 4. Mean velocity profiles (top) and Turbulent viscosity profiles (bottom) predicted using SA model for a three dimensional domain.

The predicted nondimensional velocity profiles, Figure 5, using the standard $k-\varepsilon$ model showed higher values near the channel center than what was predicted with the SA turbulence model. Figure 5 shows three different results obtained with the standard $k-\varepsilon$ model: the '$k-\varepsilon$' legend represents the results obtained from the model with the wall functions as described previously, '$k-\varepsilon$ wf pot source' utilized the wall function in calculating the source term in the electric potential, and '$k-\varepsilon$ set pot grad' results were obtained using the same electric potential that was obtained from the SA simulations. These three cases were included in order to assess the sensitivity of the simulations to the calculation of the electric potential. It is important to accurately capture the gradient of the velocity field (Eq.(5)) but this imposes a problem when meshes designed for wall functions are used. Figure 6 shows that indeed the gradient of the potential is significantly underestimated without good wall layer resolution. One way to capture the velocity gradient is to use finer meshes (resolving the viscous and the buffer layer) but this does not serve the purpose of the present study.

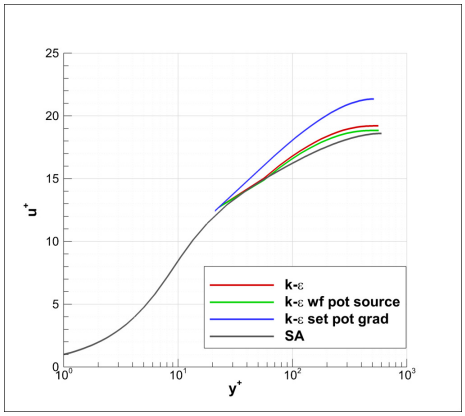

Figure 5. Mean velocity profiles predicted using standard $k-\varepsilon$ turbulence model; Ha=20, Re=1e4.

It was decided to explore the results from the $k-\varepsilon$ model if the electric potential equation was not solved, but instead prescribed as calculated from a well resolved simulation using SA model.

The electric potential gradient used in the simulations was taken at the middle of the domain ($z/H = 0$) because it is far away from the walls in the z-direction and can be analogous to a two dimensional simulation ($d\varphi/dx = 18.3$ [V/m]). As shown in Figure 5 the calculations using a fixed potential gradient ($k-\varepsilon$ set pot grad) predicted a higher value of the u^+ velocity at the center of the domain. These values were higher than what the SA model predicted, but in good agreement with the wall functions used. For a case with Re =10,000 and Ha = 20, the ratio $Ha^2/\mathrm{Re} = 4e-2$ produces values of u^+ higher than 20 as it can be seen in Figure 1.

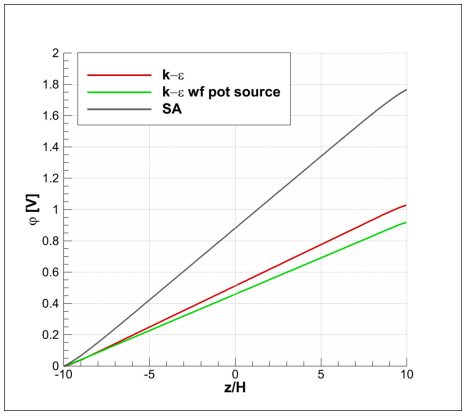

Figure 6. Variation of electric potential in the z-direction.

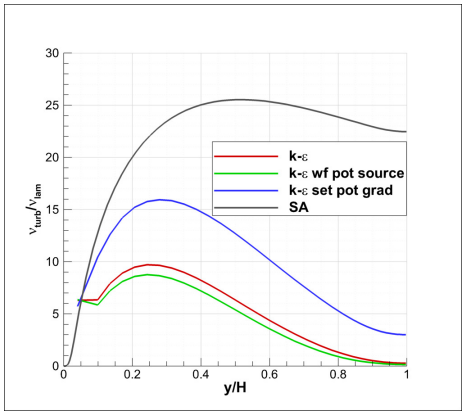

Figure 7. Turbulent viscosity profiles predicted using standard $k-\varepsilon$ turbulence model.

The calculated profiles using the $k-\varepsilon$ turbulence model followed the v_t/v trend of the SA calculation but the values were under-predicted (Figure 7). Much better results were obtained by prescribing an accurate electric potential field showing the importance of capturing the gradient of the electric potential calculation near the wall.

Figure 8 shows the turbulent kinetic energy and turbulent dissipation profiles obtained from the $k-\varepsilon$ calculations. It can be seen that the turbulent kinetic energy is higher near the center for the case where the electric potential was fixed; hence a higher turbulent viscosity ratio near the center.

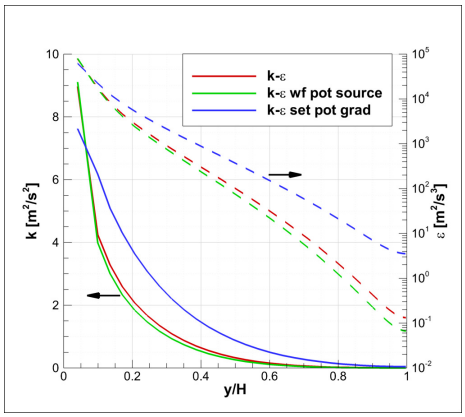

Figure 8. Turbulent kinetic energy and turbulent dissipation rate profiles predicted using standard $k-\varepsilon$ turbulence model.

Two dimensional results

The two dimensional simulations were performed in the domain shown in Figure 9. Non uniform meshes were used for all cases, the first cells from the wall was always at the same y^+ distance and the refinement was performed in the interior of the domain with finer mesh near the symmetry boundary condition (y/H = 1).

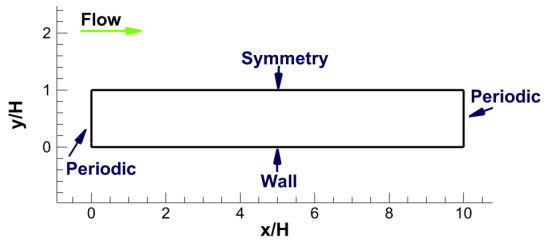

Figure 9. Two dimensional domain and boundary conditions.

The calculations were performed for the case of Ha = 20 and 54. These simulations, as discussed previously, did not solve the electric potential instead the value of the potential gradient was prescribed from the three dimensional SA simulations. Figure 10(a) shows the nondimensional mean velocity profiles calculated using the standard $k-\varepsilon$ turbulence model with wall functions. The simulations correspond for a non-uniform mesh with 128 computational cells in the y-direction.

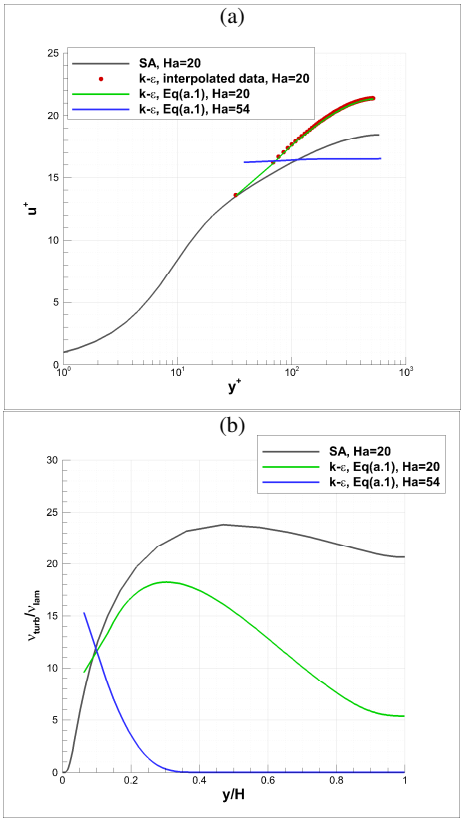

Figure 10. The velocity profiles (top) turbulent viscosity profiles (bottom) in two dimensional cases for 128 cells: Ha = 20 and Ha = 54 with Re=1x10^4.

Mean velocity profiles shown in Figure 10(a) are very similar to the three dimensional case with fixed potential gradient shown in Figure 5 indicating that the wall function approach works reasonably well. The difference between these two approaches in terms of (v_t / ν) can be seen in Figures 7 and 10(b).

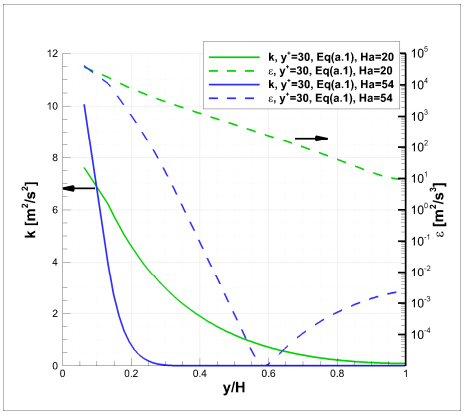

Figure 11. Turbulent kinetic energy and turbulent dissipation rate profiles predicted using standard $k-\varepsilon$ turbulence model, Ha = 20.

Figure 11 shows the turbulence calculations predicted by the two dimensional domain. These results can be directly compared with Figure 8. The slight differences in the turbulent kinetic energy profiles have a noticeable impact on the turbulent viscosity ratio due to its dependency on the square value of the kinetic energy variable.

Results shown in Figures 10 and 11 for Ha = 54 ($Ha^2/Re = 0.29$) indicate that the flow is either laminar or in the transitional regime. This was also confirmed by the results of the SA model predicted nearly zero ν_{turb} (not shown).

CONCLUSIONS

CFD simulations of MHD turbulent channel flow were performed using two different turbulence models, SA and the standard $k-\varepsilon$ focusing on cases with a prescribed constant magnetic field which resulted in a negative Lorentz force. Since the SA model yielded results in fairly good agreement with the DNS results with or without good wall resolution they were used to assess the performance of the proposed wall functions.

Standard $k-\varepsilon$ simulations were performed for three and two dimensional domains. Results showed that the electric potential gradient was being under predicted, for this reason it was decided to use the electric potential gradient that was obtained from the SA simulations that fully resolved the turbulent boundary layer. This enabled two dimensional simulations using the standard $k-\varepsilon$ model with a prescribed electric potential gradient.

Empirical functions for the velocity profile were formulated as a hybrid construct of the standard log-law and a hyperbolic tangent profile which is suitable for large Hartman number cases. The dimensionless number $\xi = Ha^2/Re$ is found to be an appropriate scaling factor in the empirical correlations.

Simulations were performed first with using the discretized velocity data reported in Kenjeres and Hanjalic (2004). This was done to minimize the errors that would arise from empirical functions. Then the same simulations were repeated using the empirical functions and shown that indeed the proposed functions do work in conjunction with the application of standard $k-\varepsilon$ model such that $y^+(1) > 20$ provided that an accurate electrical potential gradient is prescribed. Unfortunately such accuracy cannot be achieved without fine grid resolution in the wall layer. The development of semi-analytical functions for the electric potential in the wall layer is a topic for future study.

This analysis has also shown that the flow becomes laminar under the action of negative (adverse) Lorentz force at about $Ha^2/Re > 0.30$; when this ratio is less than 0.15 it can be considered to be in fully turbulent regime, and being transitional in between.

ACKNOWLEDGEMENT

This work was partially funded by US DOE National Energy Technology Laboratory (NETL) (Activity #: 4000.2.600.232.002).

APPENDIX A

We approximate the velocity profile with the following hybrid function.

$$u^+ = \lambda \frac{1}{\kappa} \ln(Ey^+) + (1-\lambda)\beta \tanh(\alpha y^+) \qquad (a.1)$$

$$\lambda = 0.5A(\xi)\{1 + \tanh[(\gamma(y - y_0))]\} \qquad (a.2)$$

$$A(\xi) = 0.5a\{1 - \tanh\{b[(\ln(\xi) + 2]\}\} \qquad (a.3)$$

where α and β are parameters to be evaluated, $\xi = H_a^2 / \mathrm{Re}$, $\gamma = 0.1$, $a = 1.1$, $b = 4.0$, and $y_0 = 30.0$. α and β are determined using a nonlinear least square curve fit to the digitized data for Ha range ($0 \sim 400$). The fitted curves and the mean velocity profiles at different magnetic field intensities are shown in Figure a-1; α and β values are listed in Table a-1. Note that $\lambda \cong 1.0$ and need not be a funcion of y^+ for wall function applications when $y^+(1) > 60$.

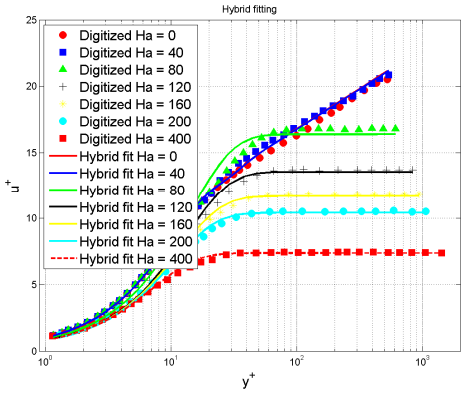

Figure a-1. Fitted velocity profiles at different magnetic field intensities to the digitized data from Kenjeres et al. (2004). Re=2.2E4.

Table a-1. Values of α and β from curve fitting of digitized data via nonlinear least square schemes.

Ha	Ha^2/Re	alpha	beta
0	0.00E+00	0.07457	13.14
40	7.27E-02	0.0754	13.07
80	2.91E-01	0.05332	16.38
120	6.55E-01	0.05746	13.54
160	1.16E+00	0.06597	11.69
200	1.82E+00	0.07301	10.42
400	7.27E+00	0.106	7.37

REFERENCES

Chaudhary, R., Shinn, A. F., Vanka, S. P., and Thomas, B.G., 2011, "Direct Numerical Simulations of Transverse and Spanwise Magnetic Field Effects on Turbulent Flow in a 2:1 Aspect Ratio Rectangular Duct", *Computers and Fluids*, Vol. 51, pp. 100-114.

Chen, Z., Zhang J., and Lee C., 2010, "Direct numerical simulation of the turbulent MHD channel flow at low magnetic Reynolds number for electric correlation characteristics", *Science China Physics, Mechanics and Astronomy*, Vol 53, pp. 1901-1913.

Dieteker, J. F., and Hoffmann, K. A., 2003, "Modified One-Equation Turbulence Models for Turbulent Magnetohydrodynamic Flows", *Journal of Thermophysics and Heat Transfer,*Vol. 17, pp. 509-520.

Kenjeres, S., Hanjalic, K., Bal, D., 2004, "A DNS-Based Second-Moment Closure for Turbulent MHD Flows", *Physics of Fluids,* Vol 16, pp. 1229-1241.

Kobayashi, H., Shionaya, H., and Okuno, Y., 2012, "Turbulent Duct Flows in a Liquid Metal Magnetohydrodynamic Power Generator", *Journal of Fluid Mechanics*, Vol. 713, pp. 243-270.

Launder, B. E., and Spalding, D. B., 1972, "Lectures in Mathematical Models of Turbulence" *Academic Press*, London, England.

Lee, D., and Choi, H., 2001, "Magnetohydrodynamic Turbulent Flow in a Channel at Low Magnetic Reynolds Number", *Journal of Fluid Mechanics*, Vol. 439, pp. 367-394.

Noguchi, H., and Kasagi, N., 1994, "DNS of Liquid Metal MHD Turbulent Channel Flows", *JSME,* Vol. 365, pp. 940-53 (in Japanese).

Pope, Stephen B., 2000, *Turbulent flows*. Cambridge university press.

Takahashi, M., Inoue, A., Aritomi, M., and Matsuzaki, M., 1989, "Numerical Analysis for Laminar and Turbulent Liquid-Metal Flow in a Transverse Magnetic Field", *Fusion Engineering and Design*, Vol. 8, pp. 249-256.

Versteeg, H.K., and Malalasekera, W., 2007, "An Introduction to Computational Fluid Dynamics: The Finite Volume Method", *Pearson-Prentice Hall*, Second Edition, Essex, England.